



HAL
open science

Failure modes of silicon heterojunction photovoltaic modules in damp heat environment : Sodium and moisture effects

Lucie Pirot-Berson, Romain Couderc, Romain Bodeux, Julien Dupuis

► To cite this version:

Lucie Pirot-Berson, Romain Couderc, Romain Bodeux, Julien Dupuis. Failure modes of silicon heterojunction photovoltaic modules in damp heat environment : Sodium and moisture effects. *Solar Energy Materials and Solar Cells*, 2024, 278, pp.113190. 10.1016/j.solmat.2024.113190 . cea-04747244

HAL Id: cea-04747244

<https://cea.hal.science/cea-04747244v1>

Submitted on 21 Oct 2024

HAL is a multi-disciplinary open access archive for the deposit and dissemination of scientific research documents, whether they are published or not. The documents may come from teaching and research institutions in France or abroad, or from public or private research centers.

L'archive ouverte pluridisciplinaire **HAL**, est destinée au dépôt et à la diffusion de documents scientifiques de niveau recherche, publiés ou non, émanant des établissements d'enseignement et de recherche français ou étrangers, des laboratoires publics ou privés.

1 <https://doi.org/10.....> DOI placeholder (WILL BE FILLED IN BY TIB Open Publishing)

2 © Authors. This work is licensed under a [Creative Commons Attribution 4.0 International License](https://creativecommons.org/licenses/by/4.0/)

3 Published: (WILL BE FILLED IN BY TIB Open Publishing)

4 **Failure modes of silicon heterojunction photovoltaic** 5 **modules in damp heat environment: sodium and** 6 **moisture effects**

7 Lucie Pirot-Berson^{1,2} [<https://orcid.org/0009-0003-2593-5849>]*, Romain Couderc¹ [<https://orcid.org/0000-0002-8696-6361>],
8 Romain Bodeux² [<https://orcid.org/0000-0001-7182-5083>], Julien Dupuis³ [<https://orcid.org/0000-0002-2051-3079>]

9 ¹Univ Grenoble Alpes, CEA, LITEN, DTS, INES, F-38000, Grenoble, France

10 *E-Mail: lucie.pirot-berson@cea.fr

11 ²EDF R&D – IPVF, 18 boulevard Thomas Gobert, 91190 Palaiseau, France

12 ³EDF R&D, EDF Lab Les Renardières, Avenue des Renardières, 77250 Moret Loing et Orvanne, France

13 **Abstract.**

14 Silicon heterojunction (SHJ) solar cells are expected to gain significant market share in the
15 coming years. In the field, among identified degradation modes, moisture-induced degradation
16 can be a significant concern for this solar cell technology and should be monitored. This work
17 investigates the moisture-induced degradation mechanisms in SHJ cells encapsulated in dif-
18 ferent module configurations. Damp heat (DH) testing was performed under IEC 61215 stand-
19 ard conditions (85 °C and 85% relative humidity) for up to 2000 h. Different degradation mech-
20 anisms are identified after DH aging, due to moisture alone or in combination with sodium ions
21 originating from photovoltaic glass leaching. Under the influence of moisture, these ions can
22 migrate into the cell and degrade the cell passivation, resulting in massive power losses up to
23 57.6% of the initial value after 1500 h of DH aging. By using other types of glass, glass-glass
24 module configurations show less than 3% of power losses after 2000 h of DH aging. The front
25 side of the cell is much more sensitive than the rear side where the emitter of the cell is. After
26 highlighting the impact of sodium, moisture alone was studied with a module configuration
27 without glass. In that case, the degradation is characterized by increased series resistance
28 without passivation losses.

29 **Keywords:** SHJ solar cells, sodium, humidity-induced degradation, leaching, reliability, TCO.

30

31 1 Introduction

32 Silicon heterojunction (SHJ) solar cells are expected to reach 20% of the world market share
33 by 2034 [1]. This technology allows very high efficiencies, with a world record of 26.81% and
34 27.09% with front and rear contacts respectively [2], [3], thanks to the good passivation of the
35 crystalline silicon (c-Si) surface by intrinsic hydrogenated amorphous silicon ((i) a-Si:H) [4]. On
36 top of cell, transparent conductive oxide (TCO) layers are deposited on both sides of the cell
37 with a dual function: as an electrode for laterally conducting carriers and as an antireflection
38 coating (ARC). In addition to cell performance, photovoltaic (PV) modules should continue to
39 produce more than 80% of their initial output for at least 25 years [5]. From a literature survey
40 of 54 performance datasets, Arriaga Arruti et al. calculated a median and average performance
41 loss rate (PLR) of 0.56%/year and 0.7%/year respectively, due to encapsulant discoloration,
42 loss of cell passivation, water ingress, potential-induced degradation (PID) and UV exposure
43 [6]. In the PV industry, the damp heat (DH) test is used to check the sensitivity of a module to
44 long-term exposure to moisture. It consists of exposing the module to an environment of 85 °C
45 and 85% relative humidity (RH) for 1000 h. After this exposure, the module must loss less than
46 5% of its maximum power to pass the test defined by the IEC 61215 protocol [7]. To surpass
47 these criteria, an understanding of the mechanisms is required. Recently, several studies have
48 shown the important sensitivity of SHJ modules to moisture, presenting new modes of degra-
49 dation that still need to be unveiled [8], [9], [10].

50 These works pointed to the soda-lime glass as the source of degradation, and in par-
51 ticular, the sodium ions (Na⁺) contained in this type of glass. In fact, the soda-lime glass is the
52 main glass used for module encapsulation due to its low cost and high availability [11]. It is
53 well known in the PV industry that under a strong electric field between the cell and the module
54 frame, sodium ions can be extracted from the glass and migrate towards the cell, leading to
55 PID [12]. However, in the absence of a voltage bias, soda-lime glass is also known to leach
56 and release sodium ions in contact with moisture [13], [14]. Once released from the glass
57 surface, these ions can diffuse within the encapsulant towards the cell.

58 At the cell level, several studies have investigated the effect of these sodium ions on
59 SHJ cells. In these works, the sodium source is artificially added by dropping a droplet or by
60 spraying uniformly different types of water solutions with sodium onto the cell surface. For the
61 remainder of this article, we will refer to these tests as accelerated sodium tests. Adachi et al.
62 used droplets of 0.05 wt% NaHCO₃ aqueous solution and obtained photoluminescence (PL)
63 signal losses on droplet areas after 3 h of DH testing showing the loss of passivation [8]. Gnoc-
64 chi et al. dropped NaOH droplets with different concentrations and presented PL signal losses
65 on droplet areas after 4 h of DH exposure [10]. After 24 h, the PL signal is completely lost,
66 even outside the droplet zones. Other studies have extended the test to the entire cell by
67 spraying water solutions over the entire cell surface, always followed by DH exposure. Li et al.
68 sprayed a 0.2 wt% NaHCO₃ solution on the front and rear of entire cells before 18 h of DH
69 aging. They observed degradation of TCO films with chemisorption of Na⁺ and H₂O in grain
70 boundaries and acceleration of the In₂O₃ decomposition due to the Na⁺ presence [15]. In their
71 next study, they showed diffusion of these species into the (i) a-Si:H film, degrading the pas-
72 sivation of the cell [16]. Sen et al. used a NaCl (0.9 wt%) solution and sprayed it on either the
73 front side, the rear side or both sides of the cell, followed by 20 h of DH exposure [17]. After
74 this artificial exposure, they observed an increase in the contact resistance from the metalliza-
75 tion of both sides of SHJ cells. They suggested that sodium and chloride ions penetrated the
76 metal contacts, leading to a weakening of the adhesive strength at the interface between the
77 metal contact and the silicon substrate. In a more recent paper, they suggested that this con-
78 tact degradation could increase its porosity, leading to a reduction in carrier collection efficiency
79 [18]. Finally, several mechanisms of SHJ cell degradation have been proposed, but they do
80 not point to the same causes, so further investigation is needed and the representativeness of
81 the accelerated sodium tests needs to be confirmed.

82 Previous works mentioned the detrimental impact of sodium ions on SHJ modules.
83 Adachi et al. compared glass-backsheet modules with soda-lime glass and with Na⁺-free glass
84 after 1000 h of damp heat test [8]. The soda-lime glass configuration showed 11% of maximal
85 power (P_{max}) degradation after the test compared with the sodium-free glass configuration that
86 shows only 1% of P_{max} losses. Sen et al. identified four failure modes for SHJ glass-backsheet
87 modules linked to chemical reactions between several contaminants (introduced to the cells
88 during handling or characterization before encapsulation), moisture and the module compo-
89 nents such as soldering flux, ribbon wire, silver paste, indium tin oxide (ITO) layers and eth-
90 ylene-vinyl acetate (EVA) films [19], without mentioning any sodium effect. Gnocchi et al. ob-
91 served significant degradation (65% of P_{max} losses) of SHJ glass-glass modules after 2000 h
92 of DH aging compared to passivated emitter and rear contact (PERC) modules with the same
93 glass and encapsulant that only showed slight degradation [10]. By testing different configura-
94 tions (glass-glass modules, polymer encapsulation only, no encapsulation), they identified the
95 glass as the main root cause of SHJ module degradation. More recently, they proposed a
96 detailed microscopic model of moisture-induced degradation in SHJ modules with EVA encap-
97 sulation [10]. In their PID study, Arriaga Arruti et. al observed more than 20% of P_{max} degra-
98 dation for their unbiased glass-backsheet modules after only 500 h of DH exposure [20].

99 This work aims to investigate the degradation mechanisms of silicon heterojunction
100 modules under damp heat environment. The goal is to extend the cell study to module scale,
101 taking into account all parameters. By using soda-lime glass, the sodium source is not artificial
102 (unlike sodium water solution) and allow to get closer to the real amount of sodium in the
103 module. The process of glass lixiviation, sodium and moisture migration and hydration in the
104 encapsulant layer are taken into account in this work. Six module configurations are tested to
105 understand the role of sodium and moisture on SHJ modules, and their combination. Soda-
106 lime glass modules are compared to borosilicate glass and strengthened glass with potassium.
107 The frontsheet-backsheet configuration is used to evaluate the effect of moisture alone without
108 any source of sodium. Finally, the frontsheet-glass and glass-backsheet configurations provide
109 information on the sensitivity of the front and rear sides of the cell and the different migration
110 mechanisms in the module.

111 2 Experimental details

112 2.1 Solar cells and modules preparation

113 For SHJ cell preparation, 160 μm -thick M2 n-type wafers were used. Passivation layers (i) a-
114 Si:H were deposited on both sides and selective layers (n) a-Si:H and (p) a-Si:H on front and
115 rear side respectively. These layers were deposited using industrial plasma-enhanced chemi-
116 cal vapor deposition (PECVD) equipment. Then, 100 nm-thick TCO layers were deposited us-
117 ing a physical vapor deposition (PVD) equipment. For the front side, an indium tin oxide (ITO)
118 with a 97/3 wt% $\text{In}_2\text{O}_3/\text{SnO}_2$ composition was used. For the rear side, an industrial "SCOT"
119 product from Advanced Nano Products was used, which is a hydrogenated indium oxide based
120 material. They have a sheet resistance R_{sheet} of 98 and 55 Ω/sq , an electron concentration of
121 $1.40 \times 10^{20} \text{ cm}^{-3}$ and an electron mobility of 27.7 and 55.6 $\text{cm}^2\text{V}^{-1}\text{s}^{-1}$, respectively. The cell ar-
122 chitecture is shown in Figure 1.

123
124
125
126
127
128

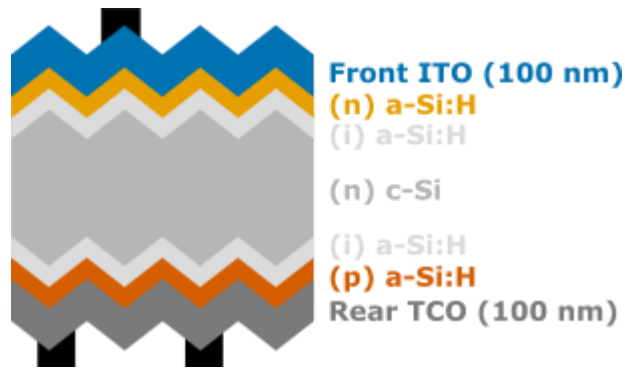
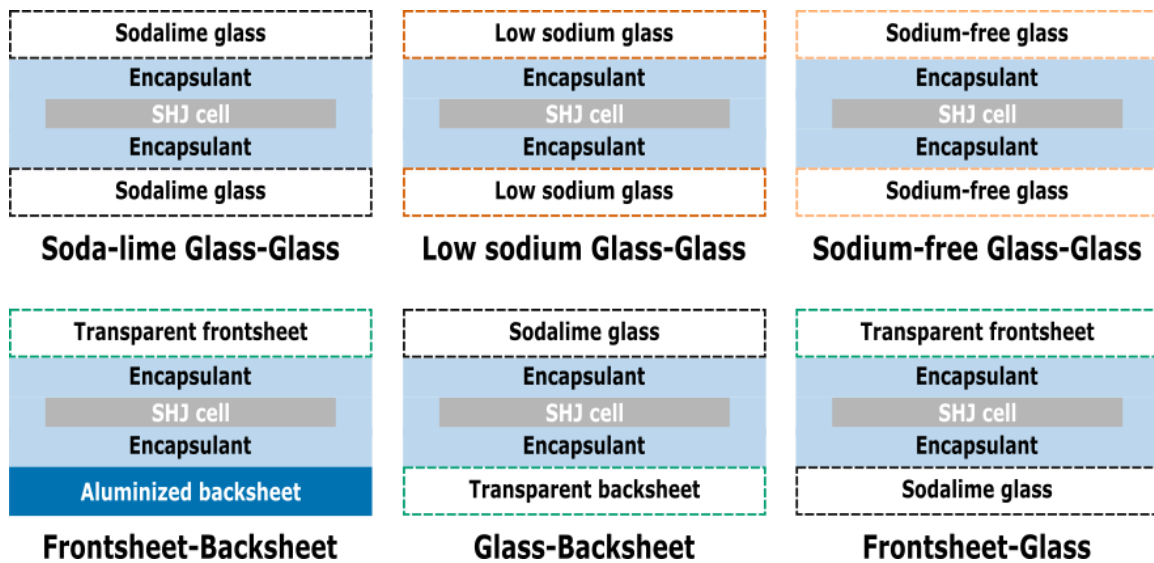


Figure 1 Scheme of n-type heterojunction solar cell with rear-emitter and different TCO layers between front and rear sides.

129 After production, the cells were cut in half with an IR laser (without edge passivation) and were
130 interconnected in pairs with ribbons and pads of electrically conductive adhesive (ECA) to form
131 strings of two half-cells. For module production, the polymer encapsulant used was a thermo-
132 plastic polyolefin with a high water absorption coefficient and a water vapor transmission rate
133 (WVTR) greater than 4 g/m².day at 23 °C and 85%RH. This material was chosen to enhance
134 the migration of moisture and ions and to better highlight the degradation mechanisms.

135 Five types of materials for module covers were used to produce six different module
136 configurations, as shown in Figure 2 with three types of glass: soda-lime glass containing so-
137 dium (~17%mol Na₂O), borosilicate low sodium glass (<4%mol of Na₂O) and sodium-free
138 glass (with K₂O instead of Na₂O). Two types of polymer films were used: an opaque aluminized
139 backsheet and a transparent film used as frontsheets or backsheets.



140
141
142

Figure 2 Six configurations of SHJ modules with same SHJ cells and encapsulant layers but different covers.

143 Eighteen modules (three per configuration) were manufactured in a 3S laminator at 160 °C
144 with a lamination time of 18 min. They were aged in an ESPEC DH85 chamber with standard
145 aging parameters (85 °C and 85% RH) [7].

146 To assess the module degradation, I-V curves were collected under standard test con-
147 ditions (AM 1.5G standard spectrum, 1000 W.m⁻² and 25 °C) with a Spire 5600 SPL flasher.
148 Modules are bifacial (except the frontsheet-backsheet ones), it allows to characterize them

149 with a front or a rear illumination. Photoluminescence (PL) and electroluminescence (EL) im-
 150 ages of modules were conducted during the aging with a BT Imaging equipment. All images
 151 were measured with the same parameters (exposure time = 0.2 s, injected current = 4.5 A (EL)
 152 and 1-sun illumination (PL)) and are presented with the same scale for comparison. These two
 153 measurements provide information on the structural and electrical degradation of the cell and
 154 module. For EL, carriers are generated by injecting current into the module. In this case, a dark
 155 area can correspond to different kinds of degradation. It can come from resistive losses that
 156 limits the injected current or it can be depassivated areas that favor non radiative recombi-
 157 nations instead of radiative ones. For PL, the carriers are generated by exposure to light thanks
 158 to the photovoltaic effect. In this case, a dark zone only corresponds to a lower quality of pas-
 159 sivation. The comparison between these two measurements therefore provides information on
 160 the type of degradation observed, and can be correlated with the I-V measurements. A New-
 161 port Oriel equipment was used to measure local external quantum efficiencies (EQE) between
 162 300 and 1200 nm with a spot size of 5 mm². The series resistances of the modules were ex-
 163 tracted from the IV measurement tool.

164 2.2 Initial module performances

165 Before aging, the glass-glass modules were subjected to I-V measurements with front illumi-
 166 nation to identify the effect of the different types of glass on the initial performances. As shown
 167 in Table 1, there are slight differences (less than 2%) between the short circuit current (I_{sc}) of
 168 the different module types, due to glass transparency and thickness differences.

169 **Table 1** Initial parameters (short circuit current I_{sc} , open circuit voltage V_{oc} and fill factor FF)
 170 of the SHJ glass-glass modules extracted from I-V curves measured with front illumination.
 171 The mean values are shown for three modules for each configuration. Standard deviations
 172 are less than 0.5% for all values presented.

Module type	I_{sc} (A)	V_{oc} (V)	FF
Soda-lime	4.68	1.45	0.79
Low sodium	4.71	1.48	0.78
Sodium-free	4.61	1.48	0.78

173

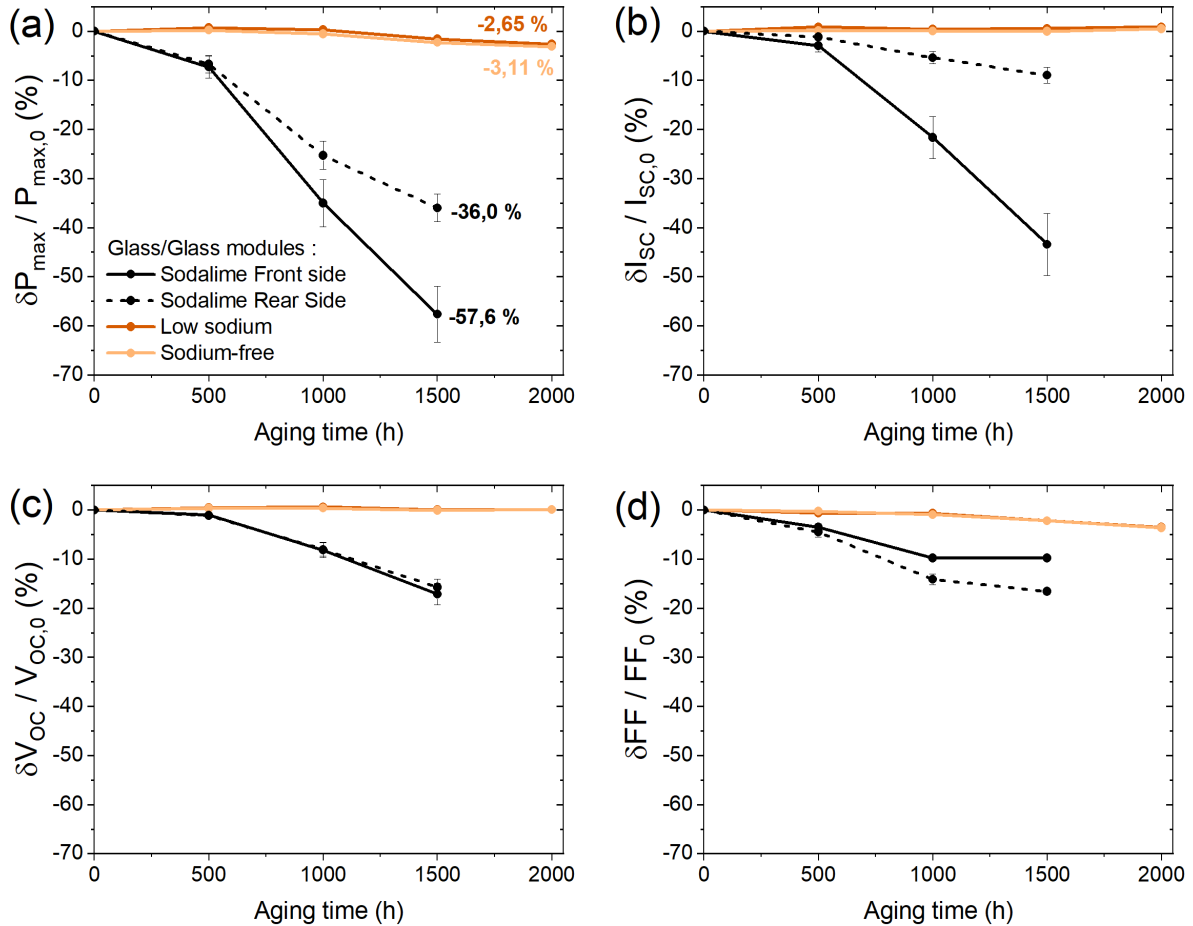
174 They have a maximum power (P_{max}) of 5.36 ± 0.05 W. The performance degradation of each
 175 type of module will be normalized to their respective initial measurements.

176 3 Results and discussion

177 3.1 Sodium-induced degradation in damp heat environment

178 Three glass-glass modules configurations were tested under DH conditions (85 °C/85% RH).
 179 Figure 3 presents the evolution of the I-V parameters of the three glass-glass SHJ module
 180 configurations during DH aging up to 2000 h with front illumination. The results with rear illu-
 181 mination are also presented for soda-lime modules.

182



183

184 **Figure 3** Evolution of the glass-glass modules P_{max} (a), I_{sc} (b), V_{OC} (c) and FF (d) during DH
 185 aging up to 2000 h. Soda-lime modules were measured with front and rear illumination. Data
 186 points represent the mean values of three identical modules and the standard deviation is
 187 shown with the error bar for each point.

188 Soda-lime modules show strong performances degradation after 1500 h of aging with approx-
 189 imately 57.6% of P_{max} losses. They are mainly due to I_{sc} losses (-43.4%) while V_{OC} and FF
 190 decrease by 17.1% and 9.76% respectively. These parameters decrease at the same rate until
 191 500 h of aging. After this time, the I_{sc} and V_{OC} reduction is significantly accelerated. The FF
 192 continues a slow decrease until 1000 h and stabilizes for the last 500 h. FF losses correspond
 193 to a notable increase ($170 \pm 27\%$) in the series resistance R_{series} (Figure S1). Regarding the
 194 results with rear side illumination, lower P_{max} losses are observed (-36.0%) compared to a front
 195 illumination. The degradation is driven by a lower I_{sc} and a higher FF reductions, while the V_{OC}
 196 losses are similar. For the modules with low sodium and sodium-free, P_{max} shows more than
 197 ten times less degradation after 2000 h of aging, respectively, 2.65% and 3.11%, correspond-
 198 ing to FF losses while I_{sc} and V_{OC} are maintained to their initial values throughout the duration
 199 of DH test. From these IV results, it is clear that the type of glass used in the module manu-
 200 facturing is of primary importance and the presence of sodium in it seems to be the source of
 201 the degradation as shown by Adachi et al., Sen et al., Li et al. and Gnocchi et al. on solar cells.

202 To reinforce the analysis that can be made of these IV results, it is important to present
 203 the spatial degradation in the modules thanks to EL and PL images of the modules. This will
 204 allow speculation on the source of the damage based on complementary characterization tech-
 205 niques. Figure 4 shows EL and PL images of one of each glass-glass module configuration every
 206 500 h during DH aging.

207



208

209 **Figure 4** EL and PL images of glass-glass SHJ modules during DH aging up to 1500 h. The
 210 images from the other modules of the same configuration are similar. They are not shown
 211 here for sake of brevity.

212 For soda-lime modules, from 500 h of aging, a reduction of EL and PL intensities (dark areas)
 213 begin to appear at the corners and edges of the module. For the next 500 h, the degradation
 214 progresses towards the center of the module, following the water ingress profile into the glass-
 215 glass module (moisture penetrates from the modules edges towards the center). After 1500 h
 216 of aging, the images are completely darkened. For the modules with low sodium or sodium-
 217 free, no significant variations in EL and PL intensities were detected after 1500 h of DH aging.

218 The EL and PL images are correlated to the IV results from Figure 3. After 500 h, I_{SC}
 219 and V_{OC} reductions are associated with the dark areas visible in the PL images localized at the
 220 modules edges (Figure 4), corresponding to the degradation of the cell passivation. First, the
 221 passivation of the dark areas in PL is reduced (V_{OC} losses), due to the sodium diffusion on the
 222 cell front and rear sides. These areas show a reduced PL intensity. Eventually, the process
 223 causing the passivation decrease ends in local I_{SC} losses, corresponding to even lower PL
 224 intensity. Compared to cell studies with the accelerated sodium test [16], these module-scale
 225 results show an evolution of the V_{OC} losses that can lead to I_{SC} losses after diffusion of sodium
 226 ions. This means that sodium ions have probably crossed the TCO layers and reached the
 227 amorphous silicon layers of the cell.

228 Simultaneously, FF losses are observed with a notable increase in the series res-
 229 sistance. This is probably due to TCO hydration with the chemisorption of OH^- in grain bound-
 230 aries, which can act as charge trapping and scattering centers and ultimately reduce the lateral
 231 conductivity of the layers [15]. This may also be due to the ECA degradation [21] or to corrosion
 232 of busbars and fingers. The presence of sodium in TCO layers could also reduce the conduc-
 233 tivity of the layer. Gnocchi et al. have recently reported similar degradations on the same cell
 234 structure (rear-emitter) with significant reductions in I_{SC} , V_{OC} and FF [10].

235 To highlight the TCO crossing of sodium ions at grain boundaries, microscopic charac-
 236 terization have been carried out. However, the transmission electron microscopy (TEM) and
 237 the associated energy-dispersive X-ray spectroscopy (EDX) performed did not prove the pres-
 238 ence of sodium in the TCOs. In order to observe the zone of interest, a focused ion beam (FIB)

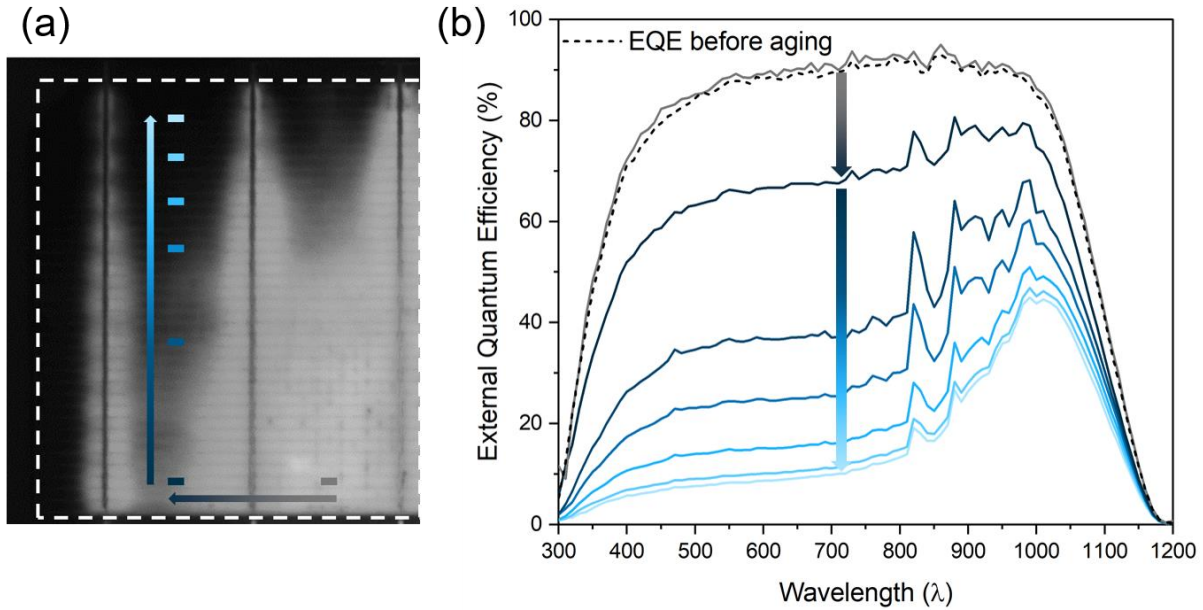
239 preparation was necessary, which implies gallium pollution of the sample. This pollution pre-
240 vented the detection of low levels of sodium because of the very close X-ray K of sodium and
241 gallium. These results suggest that the level of sodium pollution is low, even if the effect is
242 significant. In their PID study, Arriaga Arruti et al. measured sodium accumulation on the front
243 surface of the ITO layer and migration through the TCO [20]. We suggest that the main differ-
244 ence is the presence of an electric field, which is likely to result in higher sodium concentration.

245 Unlike soda-lime modules, low sodium and sodium-free modules do not show any I_{SC}
246 and V_{OC} reductions after 1500 h of aging, meaning that passivation of the cell is preserved. At
247 this time, only the soda-lime glass configuration presents growing dark areas in EL and PL
248 images, showing the significant impact of sodium in moisture-induced degradation. This vali-
249 dates the previous results published by Gnocchi et al. who measured more power degradation
250 for modules encapsulated with glass than without encapsulation [10], highlighting the signifi-
251 cant role of sodium ions .

252 For the low sodium and sodium-free modules, only FF losses remain, corresponding to
253 the action of moisture on TCO layers and contacts. In their study, Adachi et al. tested an Na^+ -
254 free glass (type not specified) and observed less degradation for these modules compared to
255 soda-lime modules [8]. Here, we demonstrate that the use of borosilicate (low sodium) and
256 potassium glass (sodium-free) as cover can be a method to avoid damp heat induced degra-
257 dation. In his work on glass lixiviation, Sterpenich has shown that sodium is more easily
258 leached than potassium, calcium and magnesium, whatever the composition of the starting
259 glass [22]. This may explain the reduced degradation of potassium glass modules.

260 After the aging test, the rear side of soda-lime modules presents lower P_{max} reduction
261 than front side (Figure 3), reflecting more degradation for the front side of the cell compared to
262 the rear side. Regarding the evolution of other parameters, the front side degradation is driven
263 by greater losses in I_{SC} compared to the rear side degradation which is driven by significant FF
264 losses. This could indicate that the front passivation is more degraded. EQE measurements
265 with front illumination were performed on these modules after 1000 h of DH aging to further
266 understand these observations.

267 Figure 5(a) displays the PL image of a soda-lime glass-glass module corner with the
268 location of 7 regions of interest for EQE measurements marked by gray and blue rectangles.
269 The blue gradient corresponds to the degradation gradient: the lighter the blue, the more de-
270 graded the area. EQE spectra obtained on each region are shown in Figure 5(b) between
271 300 nm and 1200 nm.



272

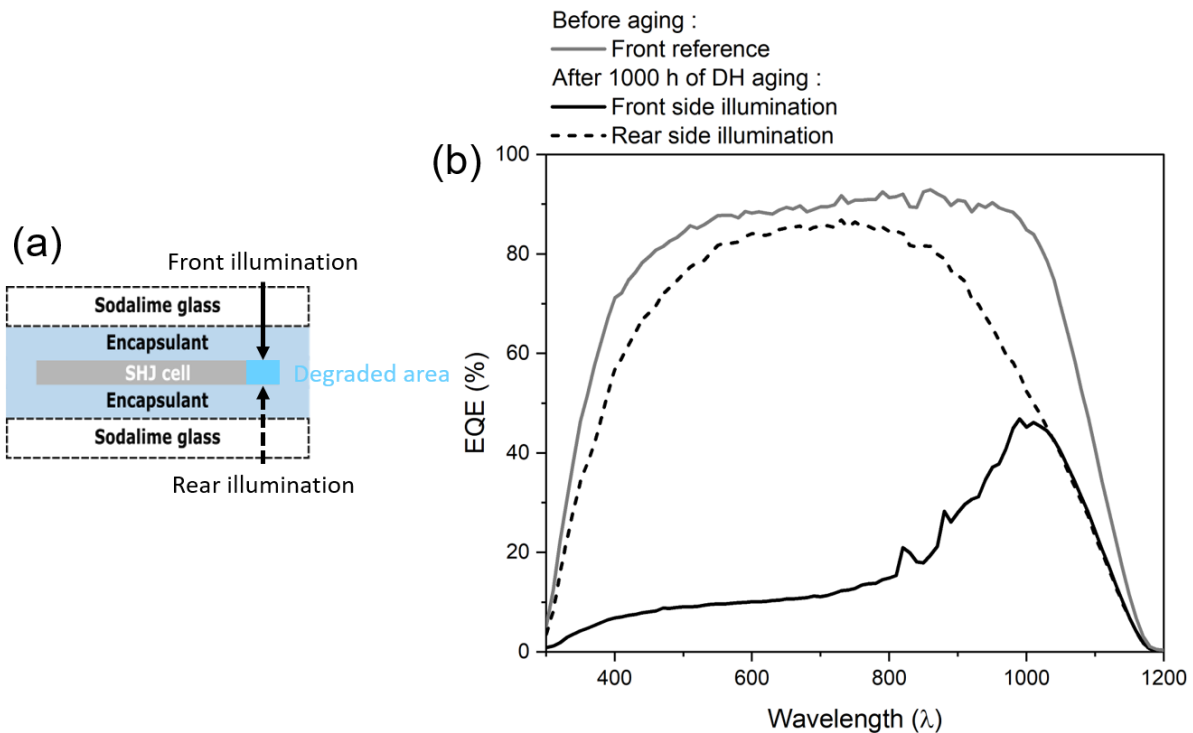
273 **Figure 5** Location of EQE measurements with front illumination after 1000 h of DH aging on
 274 soda-lime glass-glass modules (a) and results between 300 nm and 1200 nm (b). Spectrum
 275 variations between 800 nm and 1000 nm come from EQE equipment.

276 The EQE measured on the area that appears intact in the PL image (gray spot) is identical to
 277 the EQE reference measured before DH aging. The lowest EQE corresponds to the measurement
 278 point closest to the module edge, with a significant reduction for low wavelengths (300 –
 279 800 nm). The intermediate points follow the same trend with EQE reduction at low wavelengths
 280 and a decrease as they approach the edge of the module.

281 Under front illumination, short-wavelength photons are absorbed close to the front side,
 282 while photons above 800 nm are absorbed uniformly throughout the wafer's thickness [23].
 283 When the front side is altered and recombination centers are formed, electron-hole pairs obtained
 284 from short-wavelength photons have a higher probability of being recombined than photons
 285 absorbed further away from these recombination centers. Therefore these EQE results
 286 indicate high front recombination which means that the front side of cell is severely damaged.
 287 Lower EQE means lower J_{SC} and therefore I_{SC} losses. The dark areas in the PL images (Figure
 288 4) can be related to these I_{SC} losses and not only to V_{OC} losses. The lower the intensity on the
 289 PL image, the higher the I_{SC} losses. In their work, Arriaga Arruti et al. showed front-surface
 290 recombination at the edges of the cell in the case of PID degraded modules [20]. In our work,
 291 we show that the same evolution of EQE is observed after DH alone with soda-lime glasses
 292 and that EQE varies depending on the state of degradation. Diffusion of sodium atoms is sufficient
 293 to cause the observed degradation, the application of an electric field is not necessary.
 294 The intensity of the drop in EQEs progresses similarly to the progression of moisture in the
 295 module.

296 Figure 6 shows the comparison between EQE from the illuminated front and rear sides
 297 of soda-lime glass-glass modules before and after 1000 h of DH aging. Measurements are
 298 performed on the second degraded zone closest to the module edge (Figure 5).

299



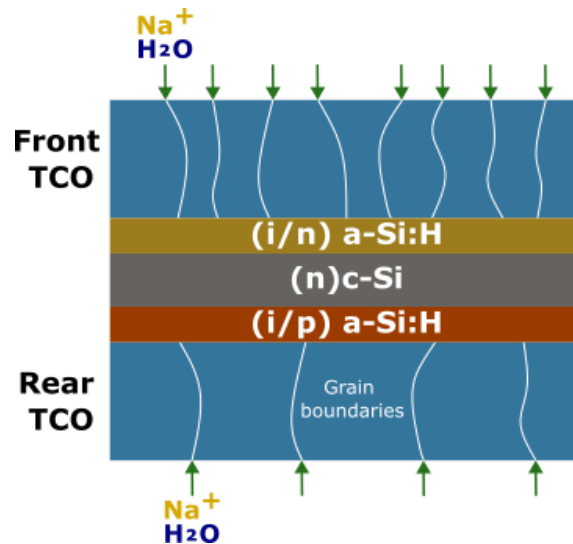
300

301 **Figure 6** Location of EQE measurements before and after 1000 h of DH aging on soda-lime
 302 glass-glass modules on the on the same degraded area with front and rear sides illumina-
 303 tion (a) and results between 300 nm and 1200 nm (b).

304 The EQE measured for the front illumination shows a significant reduction for short wave-
 305 lengths compared to the front reference. When the front passivation is degraded, the photons
 306 absorbed near the front surface are more likely to recombine before reaching the p-n junction.
 307 The EQE measured from the rear side does not show a reduction for short wavelengths but
 308 for wavelengths above 800 nm. This confirms the reduction of photon collection on the front
 309 side of the cell (the rear side with rear illumination).

310 The two differences between the front and the rear of the SHJ cells are the TCO and
 311 the a-Si layers. The front and rear TCO have the same thickness but their intrinsic properties
 312 (morphology, doping...) are different. The stack used for passivating the front surface is com-
 313 posed of a double layer of (i) and (n) a-Si:H. On the rear, a stack with (i) and (p) a-Si:H layers
 314 is used. The doping and the thicknesses are different between the front and rear regarding the
 315 (i), (n) and (p) layers. In their cell study, Jiang et. al observed significantly less stability in Na⁺
 316 environment for SHJ cells with underdense (i) a-Si:H layers, showing the predominant benefi-
 317 cial effect of using dense a-Si layers to prevent degradation in sodium environment [24]. At cell
 318 scale, Li et al. observed opposite results to ours, with greater degradation on the (p) a-Si:H
 319 side than on the (n) a-Si:H side [16], meaning that the doping type does not seem to be the
 320 parameter with the greatest impact.

321 In our case, the observed differences in degradation are probably due to the different
 322 a-Si layer density between the front and rear sides. In addition, the TCO could also have an
 323 influence on the degradation. Figure 7 shows a diagram of the SHJ cell used for these tests.
 324 The front TCO has smaller grains than the rear TCO, with sizes of 15-20 nm and 30-40 nm for
 325 front and rear sides respectively (Figure S2).



326

327 **Figure 7** Scheme of species (Na^+ and H_2O) diffusion in TCO layers of SHJ cells according to
 328 the morphology of films (not drawn to scale).

329 Small TCO grains imply a large number of grain boundaries. With more grain boundaries, the
 330 species migrations can be facilitated and the induced degradation can be accelerated. Li et al.
 331 showed the dependence of heterojunction cell stability on TCO morphology, with enhanced
 332 stability for cells with large grains of tungsten-doped indium (IWO) [15]. The doping and hydro-
 333 genation of the indium-based TCO layers could also have an effect. Note that the magnitude
 334 of the power losses caused by underdense a-Si layers presented by Jiang et al. and the low
 335 power losses reduction from increasing the TCO grain sizes by Li et al. points in the direction
 336 of a prevalence of the a-Si layers density on sodium resistance.

337

338 3.2 Impact of moisture on SHJ modules degradation

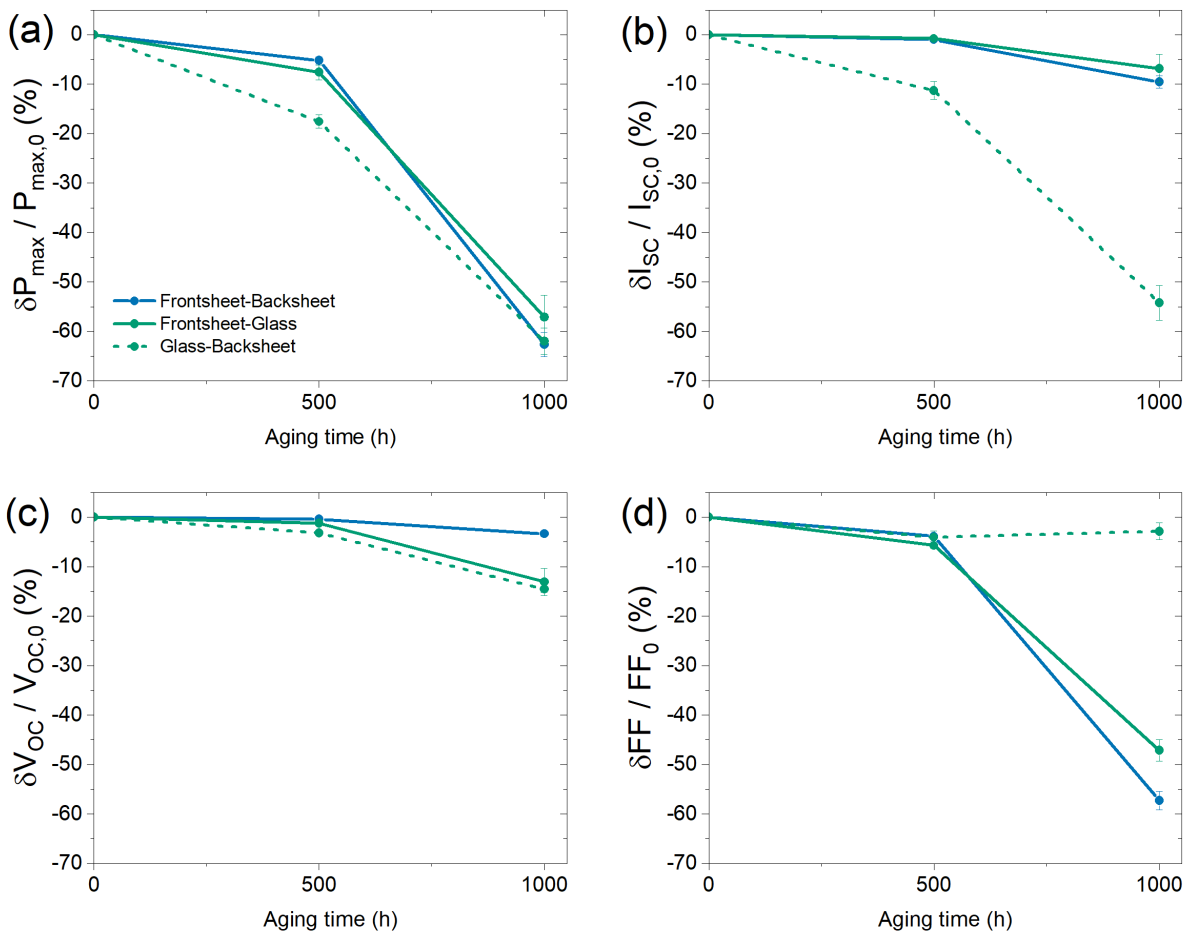
339 The first section highlighted the joint diffusion of moisture and sodium in glass-glass modules
 340 from the edges towards the center. In these modules, the quantity of moisture reaching the
 341 cells remains low compared to configurations with polymeric sheets as front and/or rear mod-
 342 ule covers. We studied three module configurations to understand the effect of each stressor
 343 (sodium and moisture) in the degradation mechanisms: frontsheet-aluminized backsheets (FS-
 344 ABS), frontsheet-glass (FS-G) and glass-backsheet (GB-S). These three configurations allow
 345 to modify the cell side (front or rear) facing the sodium source and also the main way for the
 346 moisture penetration into the module. With polymeric covers, the diffusion occurs mainly
 347 through the polymeric covers without aluminum rather than from the edges towards the center
 348 through a lateral diffusion in the encapsulant. The aluminized backsheets blocks moisture in-
 349 gress on the rear side as glass does and, at the same time, it eliminates the source of sodium
 350 in the module unlike the glass. The backsheets without aluminum and the frontsheet are the
 351 same polymeric film. These modules use the same polymer encapsulant and the same cell as
 352 in the previous section (with a front ITO and a rear indium-based TCO). As a reminder, the
 353 encapsulant is a thermoplastic polyolefin with a high water absorption coefficient and a WVTR
 354 greater than $4 \text{ g/m}^2 \cdot \text{day}$ at $23 \text{ }^\circ\text{C}$ and $85\% \text{RH}$. This material was chosen to enhance the mi-
 355 gration of moisture and ions and to better highlight the degradation mechanisms on the cell.

356 The FS-ABS configuration is used to study the effect of moisture on degradation mech-
 357 anisms without the influence of sodium. The FS-G and G-BS can be compared to evaluate the
 358 effect of moisture and sodium on both sides of the cell. Table 2 summarizes the different
 359 sources of degradation for the different configurations.

360 **Table 2** Degradation sources for the different module configurations with polymer sheets.

Side	Moisture ingress		Sodium source	
	Front	Rear	Front	Rear
Frontsheet-Aluminized Backsheet (FS-ABS)	✓	✗	✗	✗
Frontsheet-Glass (FS-G)	✓	✗	✗	✓
Glass-Backsheet (G-BS)	✗	✓	✓	✗

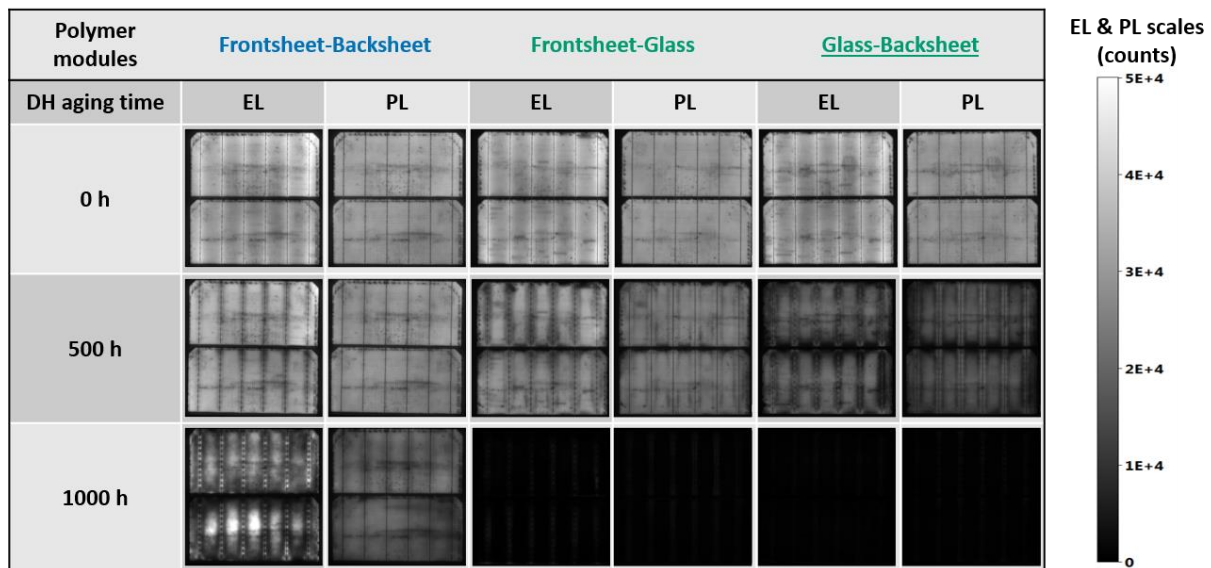
361 Figure 8 presents the evolution of the I-V parameters of these polymeric modules during DH
362 aging up to 1000 h with front illumination.



363
364 **Figure 8** Evolution of the polymeric modules P_{max} (a), I_{sc} (b), V_{oc} (c) and FF (d) during damp
365 heat aging up to 1000 h with front illumination. Data points represent the mean values of
366 three identical modules and the standard deviation is shown with the error bars.

367 After 1000 h of DH aging, FS-ABS, FS-G and G-BS modules show similar maximal power
368 degradation of 62.6%, 57.1% and 62.0% respectively. FS-ABS and FS-G show mainly FF
369 losses (57.3% and 47.1%) while G-BS have mainly I_{sc} losses (54.2%) and a stable FF . FS-
370 ABS modules present almost no V_{oc} degradation whereas FS-G have similar losses as G-BS
371 (13.1% and 14.6%).

372 To better understand the spatial degradation in the module, Figure 9 shows EL and PL
373 images of polymeric modules during DH aging.



374

375 **Figure 9** EL and PL images of FS-ABS, FS-G and G-BS modules during DH aging up to
 376 1000 h. The images from the other modules of the same configuration are similar. They are
 377 not shown here for sake of brevity.

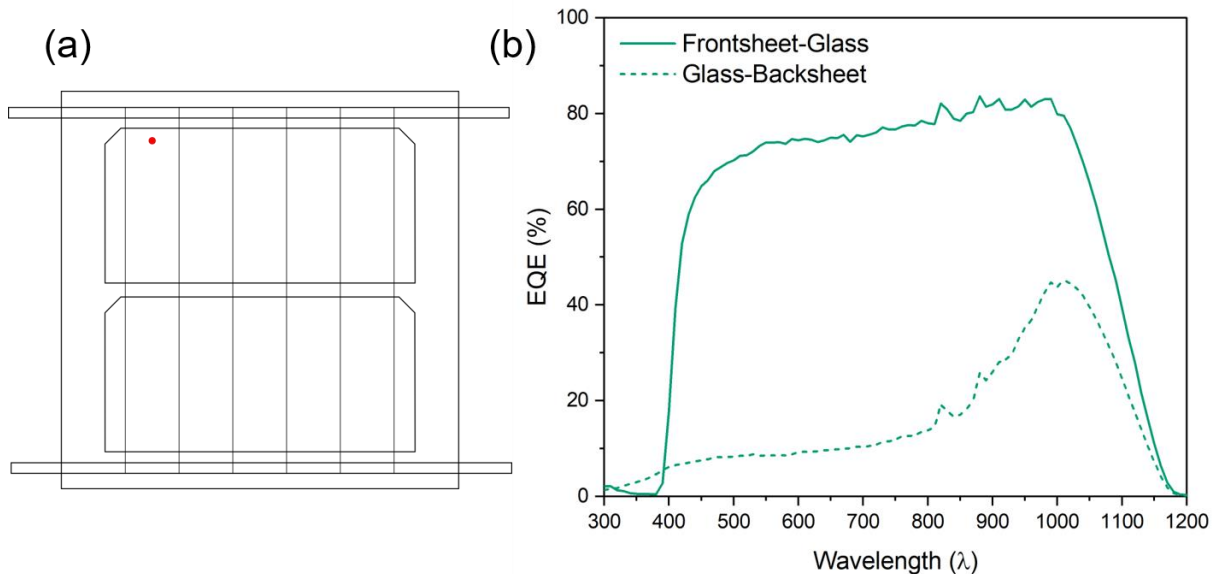
378 For the FS-ABS configuration, after 500 h of aging, dark areas appear in the EL images along
 379 the busbars and on the pads of the ECA joints. At the same time, no degradation is visible in
 380 the PL images. After 1000 h, more degradation is observed in the EL images along the busbars
 381 with larger dark areas. No dark areas are visible in the PL images, but a slight decrease in
 382 intensity is observed over the whole image. In this configuration, the moisture ingress is on the
 383 entire surface of the front side and without any source of sodium. This leads to the first degra-
 384 dation along the busbars (visible in the EL images and not in the PL images), corresponding
 385 to FF losses (Figure 8). It corresponds to an increase in the local series resistance (Figure S3).
 386 These losses can be attributed to TCO hydration, contacts corrosion and to a chemical reaction
 387 between the ECA and moisture, which can cause polymer degradation with weakening of ad-
 388hesion [25] and shear strength [26] or galvanic corrosion with increase of contact resistance
 389 [21]. Compared with soda-lime glass-glass modules, no significant drop in I_{sc} and V_{oc} is ob-
 390 served, and no totally darkened areas are visible in the PL images, showing that moisture
 391 alone does not cause cell depassivation even with much more moisture reaching the cell.

392 The FS-G configuration still has the moisture ingress on front side, but adds the sodium
 393 source on the rear side. In Figure 9, after 500 h of aging, dark areas appear in the EL images
 394 along the busbars and on the pads of the ECA joints. This corresponds to the same front
 395 degraded areas observed in the FS-ABS configuration, due to front moisture ingress. In PL
 396 images, other areas appear dark (different from those of the EL), along several millimeters
 397 away from the busbars and between the two half-cells (inter-cell area) between the busbars.
 398 This corresponds to V_{oc} losses observed after 500 h (Figure 8). These degradations are not
 399 visible for the FS-ABS configuration, which means that they are induced by the glass on the
 400 rear side. They are also not present in low sodium modules, meaning that the sodium must be
 401 present to induce these degradations. In addition, this degradation away from the busbars is
 402 not visible in the soda-lime glass-glass modules after 500 h, indicating that the front moisture
 403 ingress accelerates sodium diffusion within the FS-G modules. In PL images, we suggest that
 404 the zone of exclusion of degradation along the busbars is due to the protection provided by
 405 some ECA paste effusion. This same area is the degraded area in EL images and is respon-
 406 sible for FF losses. After 1000 h, maintaining the same scale, the EL and PL images are com-
 407 pletely darkened, indicating that the degradation has progressed across the entire module.
 408 The moisture-induced degradation on front side is the same as for the FS-ABS modules with
 409 similar moisture ingress, corresponding to contacts degradation, and is confirmed by the FF
 410 losses observed. This degradation has progressed over the entire contact areas (along the

411 busbars and on the ECA pads), resulting in an increase in series resistance caused by chem-
412 ical reactions with moisture, leading to contact degradation and corrosion. Finally, this EL in-
413 tensity reduction over the entire image is a combination between these contact degradations
414 and sodium induced degradation (PL image). At this time, after 1000 h, the sodium ions have
415 probably diffused over the entire rear side and progressed on the front side from the inter-cell
416 area, corresponding to the V_{OC} and I_{SC} losses observed (Figure 8).

417 For the G-BS configuration, similar to FS-ABS and FS-G modules, dark areas are visi-
418 ble in the EL images along the busbars and on the ECA pads after 500 h of aging. In this case,
419 the contact degradation is on the rear side due to rear moisture ingress through the backsheet
420 layer. In the PL images, dark areas are visible along several millimeters away from the busbars
421 and on the cell between the busbars, next to the inter-cell area. In this area, the moisture from
422 the rear side can reach the front glass and releases sodium ions. Then, they simply diffuse
423 over the cell front side, leading to its degradation and induced V_{OC} and I_{SC} losses. These dark
424 areas and corresponding I_{SC} losses are more significant than for FS-G modules, meaning that
425 the degradation is enhanced when the front side of the cell faces the sodium source. In the
426 FS-G configuration, the sodium ions preferentially diffuse on the rear side and must go around
427 the cell to diffuse on the front. After 1000 h, the images are completely darkened, meaning that
428 the degradation has progressed across the entire module. Compared to the FS-G modules,
429 the sodium ions have probably diffused over the entire front side and started to progress on
430 the rear side from the inter-cell area.

431 To complete these results, Figure 10(a) displays the scheme of module with the loca-
432 tion of EQE front side illumination on degraded area of FS-G and G-BS modules after 1000 h
433 of DH aging, and the associated EQE between 300 to 1200 nm in Figure 10(b).



434

435 **Figure 10** Location of EQE front side measurements with front illumination after 1000 h of
436 DH aging on polymeric modules (a) and results between 300 to 1200 nm (b).

437 The G-BS modules show lower EQE than the FS-G modules, especially for short wavelengths,
438 corresponding to front-surface recombination. For similar PL images (completely dark), the
439 EQE measurements with front illumination show the differences in degradation between the
440 two configurations. The front side of the G-BS modules is more degraded than FS-G one,
441 corresponding to the significant reduction in I_{SC} losses. These results confirm the greater im-
442 pact of sodium on the front side of the cell compared to the rear side of our modules.

443

444

445

446 Conclusion

447 This work investigates the different degradation mechanisms of silicon heterojunction modules
448 in a damp heat environment. Several module configurations were studied to vary the degrada-
449 tion sources (sodium and moisture) and their spatial distribution in the module. The modules
450 were aged under DH conditions to explore the different mechanisms that can occur. First, the
451 glass-glass configuration with soda-lime glass shows significant V_{OC} and I_{SC} losses due to de-
452 passivation of the cell with current production loss of certain areas by the action of sodium ions
453 originated from glass lixiviation. Then, by using other type of glass with low sodium or without
454 sodium, the degradation has been drastically reduced and suggest an alternative to avoid the
455 main moisture-induced degradation on SHJ cells.

456 The study shows a greater sensitivity to sodium-induced degradation of the front side
457 of the cell compared to the rear side, with significant front-surface recombination on the front
458 side. This difference may be due to the nature of the amorphous silicon layers and/or the mor-
459 phology of the TCO layers as already shown in the literature on cells.

460 The role of moisture alone was investigated by suppressing the sodium source with the
461 FS-ABS configuration or by comparing the FS-G and the G-BS configurations. After DH aging,
462 without sodium in the module, the cell passivation is maintained. However, moisture induces
463 significant FF losses, due to degradation of contacts and TCO layers which increases the se-
464 ries resistance of the modules.

465 Overall, this study shows that all material components must be considered as sources
466 of degradation and must be carefully selected to ensure module reliability. It is important to
467 notice that the mechanisms observed are specific to the cells studied in this paper and may be
468 different with different SHJ cells.

469 Data availability statement

470 The data that support the findings of this study are available from the corresponding author
471 upon reasonable request.

472 Author contributions

Author	Contribution
Lucie Pirot-Berson	Conceptualization, Data curation, investiga- tion, methodology, Formal analysis, writing – original draft
Romain Couderc	Supervision, investigation, validation, For- mal analysis, writing – review & editing
Romain Bodeux	Supervision, investigation, validation, For- mal analysis, writing – review & editing
Julien Dupuis	Supervision, investigation, validation, For- mal analysis, writing – review & editing

473 Competing interests

474 The authors declare no competing interests.

475 **Funding**

476 **Acknowledgement**

477 The authors want to acknowledge all the staff members from CEA-INES who contributed for
478 cell and module manufacturing as well as for the reliability tests. They also want to
479 acknowledge Paul Lefillastre from EDF Renewables for his expertise.

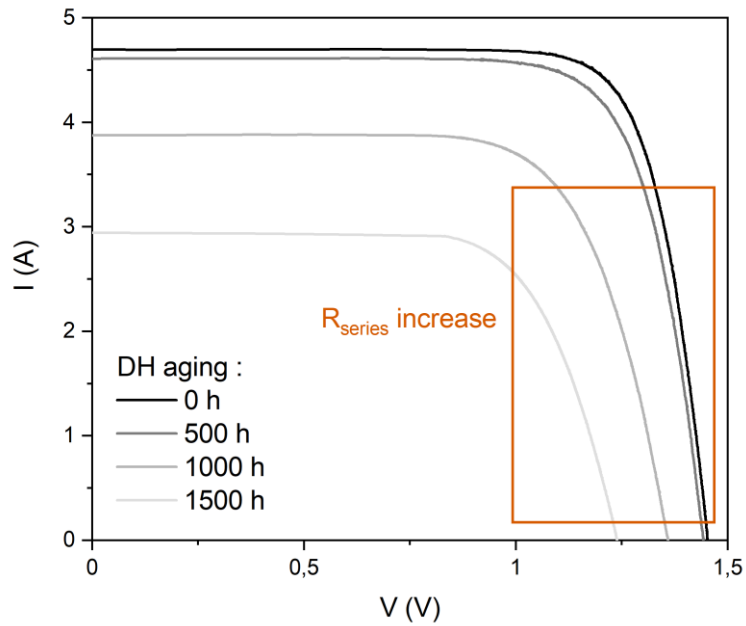
480 **References**

- 481 [1] ITRPV, "International Technology Roadmap for Photovoltaic (ITRPV): 2023 Results.,"
482 15rd edition, 2024.
- 483 [2] H. Lin *et al.*, "Silicon heterojunction solar cells with up to 26.81% efficiency achieved by
484 electrically optimized nanocrystalline-silicon hole contact layers," *Nat Energy*, vol. 8, no.
485 8, pp. 789–799, Aug. 2023, doi: 10.1038/s41560-023-01255-2.
- 486 [3] J. P. Casey, "LONGi develops heterojunction back-contact cell with record conversion
487 efficiency of 27.09%," PV Tech. Accessed: Jan. 09, 2024. [Online]. Available:
488 [https://www.pv-tech.org/longi-develops-heterojunction-back-contact-cell-with-record-](https://www.pv-tech.org/longi-develops-heterojunction-back-contact-cell-with-record-conversion-efficiency-of-27-09/)
489 [conversion-efficiency-of-27-09/](https://www.pv-tech.org/longi-develops-heterojunction-back-contact-cell-with-record-conversion-efficiency-of-27-09/)
- 490 [4] W. Liu *et al.*, "Underdense a-Si:H film capped by a dense film as the passivation layer of
491 a silicon heterojunction solar cell," *Journal of Applied Physics*, vol. 120, no. 17, p. 175301,
492 Nov. 2016, doi: 10.1063/1.4966941.
- 493 [5] I. M. Peters, J. Hauch, C. Brabec, and P. Sinha, "The value of stability in photovoltaics,"
494 *Joule*, vol. 5, no. 12, pp. 3137–3153, Dec. 2021, doi: 10.1016/j.joule.2021.10.019.
- 495 [6] O. Arriaga Arruti, A. Virtuani, and C. Ballif, "Long-term performance and reliability of sili-
496 con heterojunction solar modules," *Progress in Photovoltaics: Research and Applica-*
497 *tions*, vol. 31, no. 7, pp. 664–677, 2023, doi: 10.1002/pip.3688.
- 498 [7] "IEC 61215: Terrestrial photovoltaic (PV) modules - Design qualification and type ap-
499 proval."
- 500 [8] D. Adachi, T. Terashita, T. Uto, J. L. Hernández, and K. Yamamoto, "Effects of SiOx
501 barrier layer prepared by plasma-enhanced chemical vapor deposition on improvement
502 of long-term reliability and production cost for Cu-plated amorphous Si/crystalline Si het-
503 erojunction solar cells," *Solar Energy Materials and Solar Cells*, vol. 163, pp. 204–209,
504 Apr. 2017, doi: 10.1016/j.solmat.2016.12.029.
- 505 [9] W. Liu *et al.*, "Damp-Heat-Stable, High-Efficiency, Industrial-Size Silicon Heterojunction
506 Solar Cells," *Joule*, vol. 4, no. 4, pp. 913–927, Apr. 2020, doi:
507 10.1016/j.joule.2020.03.003.
- 508 [10] L. Gnocchi, O. A. Arruti, C. Ballif, and A. Virtuani, "A comprehensive physical model for
509 the sensitivity of silicon heterojunction photovoltaic modules to water ingress," *Cell Re-*
510 *ports Physical Science*, p. 101751, Dec. 2023, doi: 10.1016/j.xcrp.2023.101751.
- 511 [11] U. Blieske and G. Stollwerck, "Glass and Other Encapsulation Materials (Chapter 4)," in
512 *Semiconductors and Semimetals*, vol. 89, Elsevier, 2013, pp. 199–258. doi:
513 10.1016/B978-0-12-381343-5.00004-5.
- 514 [12] W. Luo *et al.*, "Potential-induced degradation in photovoltaic modules: a critical review,"
515 *Energy Environ. Sci.*, vol. 10, no. 1, pp. 43–68, Jan. 2017, doi: 10.1039/C6EE02271E.
- 516 [13] R. H. Doremus, "Interdiffusion of hydrogen and alkali ions in a glass surface," *Journal of*
517 *Non-Crystalline Solids*, vol. 19, pp. 137–144, Dec. 1975, doi: 10.1016/0022-
518 3093(75)90079-4.

- 519 [14] V. Guiheneuf, F. Delaleux, O. Riou, P.-O. Logerais, and J.-F. Durastanti, "Investigation
520 of damp heat effects on glass properties for photovoltaic applications," *Corrosion Engi-
521 neering, Science and Technology*, vol. 52, no. 3, pp. 170–177, Apr. 2017, doi:
522 10.1080/1478422X.2016.1234803.
- 523 [15] X. Li *et al.*, "Highly crystallized tungsten doped indium oxide film stabilizes silicon hetero-
524 junction solar cells in sodium environment," *Solar Energy Materials and Solar Cells*, vol.
525 233, p. 111387, Dec. 2021, doi: 10.1016/j.solmat.2021.111387.
- 526 [16] X. Li *et al.*, "Potential-free sodium-induced degradation of silicon heterojunction solar
527 cells," *Progress in Photovoltaics: Research and Applications*, vol. 31, no. 9, pp. 939–948,
528 2023, doi: 10.1002/pip.3698.
- 529 [17] C. Sen *et al.*, "Accelerated damp-heat testing at the cell-level of bifacial silicon HJT, PERC
530 and TOPCon solar cells using sodium chloride," *Solar Energy Materials and Solar Cells*,
531 vol. 262, p. 112554, Oct. 2023, doi: 10.1016/j.solmat.2023.112554.
- 532 [18] X. Wu *et al.*, "Addressing sodium ion-related degradation in SHJ cells by the application
533 of nano-scale barrier layers," *Solar Energy Materials and Solar Cells*, vol. 264, p. 112604,
534 Jan. 2024, doi: 10.1016/j.solmat.2023.112604.
- 535 [19] C. Sen *et al.*, "Four failure modes in silicon heterojunction glass-backsheet modules,"
536 *Solar Energy Materials and Solar Cells*, vol. 257, p. 112358, Aug. 2023, doi: 10.1016/j.sol-
537 mat.2023.112358.
- 538 [20] O. Arriaga Arruti, L. Gnocchi, Q. Jeangros, C. Ballif, and A. Virtuani, "Potential-induced
539 degradation in bifacial silicon heterojunction solar modules: Insights and mitigation strat-
540 egies," *Progress in Photovoltaics: Research and Applications*, vol. n/a, no. n/a, doi:
541 10.1002/pip.3765.
- 542 [21] W. Zhang *et al.*, "Electrical and mechanical reliability and failure mechanism analysis of
543 electrically conductive adhesives," *Microelectronics Reliability*, vol. 151, p. 115236, Dec.
544 2023, doi: 10.1016/j.microrel.2023.115236.
- 545 [22] J. Sterpenich, "Altération des vitraux médiévaux. Contribution à l'étude du comportement
546 à long terme des verres de confinement," phdthesis, Université Henri Poincaré - Nancy
547 1, 1998. Accessed: May 14, 2024. [Online]. Available: [https://hal.univ-lorraine.fr/tel-
548 01748127](https://hal.univ-lorraine.fr/tel-01748127)
- 549 [23] W. J. Yang, Z. Q. Ma, X. Tang, C. B. Feng, W. G. Zhao, and P. P. Shi, "Internal quantum
550 efficiency for solar cells," *Solar Energy*, vol. 82, no. 2, pp. 106–110, Feb. 2008, doi:
551 10.1016/j.solener.2007.07.010.
- 552 [24] K. Jiang *et al.*, "Balance of efficiency and stability of silicon heterojunction solar cells,"
553 *Solar Energy Materials and Solar Cells*, vol. 243, p. 111801, Aug. 2022, doi: 10.1016/j.sol-
554 mat.2022.111801.
- 555 [25] R. A. Gledhill and A. J. Kinloch, "Environmental Failure of Structural Adhesive Joints,"
556 *The Journal of Adhesion*, vol. 6, no. 4, pp. 315–330, Jan. 1974, doi:
557 10.1080/00218467408075035.
- 558 [26] S. St. Lawrence, J. L. Willett, and C. J. Carriere, "Effect of moisture on the tensile prop-
559 erties of poly(hydroxy ester ether)," *Polymer*, vol. 42, no. 13, pp. 5643–5650, Jun. 2001,
560 doi: 10.1016/S0032-3861(00)00836-3.
- 561

562 **Supplementary information**

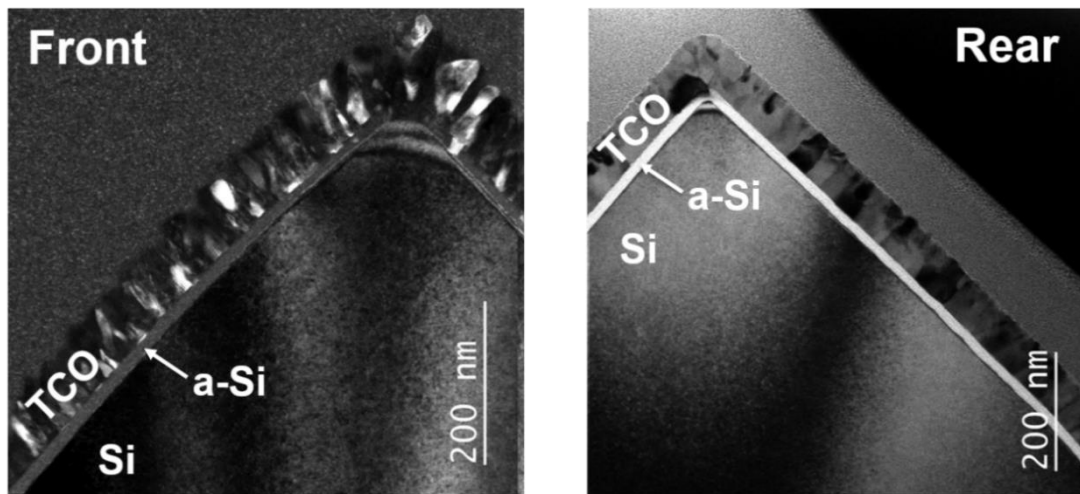
563



564

565

Figure S1 I-V curve evolution of soda-lime modules during DH aging.

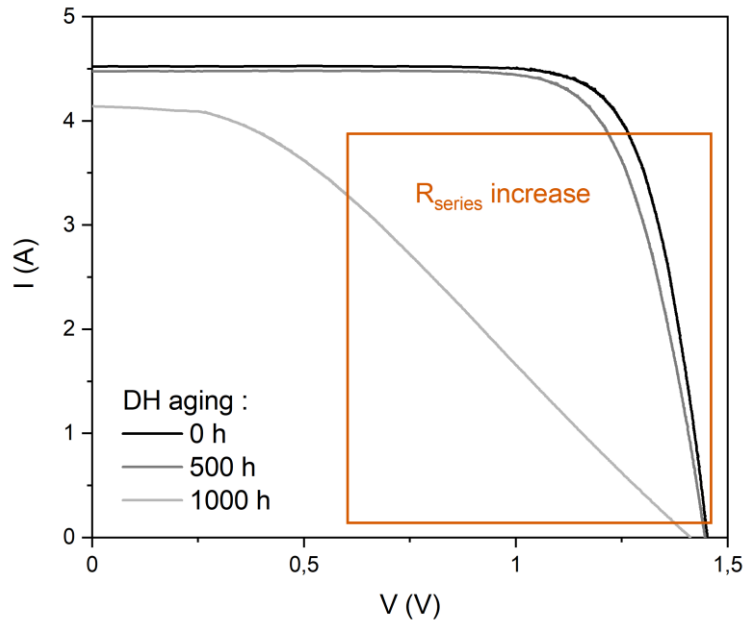


566

Figure S2 Transmission electron microscope (TEM) images of TCO layers for the front and rear side of the SHJ cells with the grain size for each side: 15-20 nm and 30-40 nm for front and rear sides respectively.

570

571



572

573

Figure S3 I-V curve evolution of FS-ABS modules during DH aging.

574

575

576